Molecular Dynamics Simulations of Reactions between Molecules: High-Energy Particle Bombardment of Organic Films

Ramona S. Taylor and Barbara J. Garrison*

Department of Chemistry, 152 Davey Laboratory, The Pennsylvania State University, University Park, Pennsylvania 16802

Received December 7, 1994. In Final Form: February 1, 1995[⊗]

The high-energy particle bombardment of a molecular film adsorbed upon a metal substrate has been investigated via molecular dynamics computer simulations with an empirical many-body potential energy function constructed for studying reactive dynamics. The specific system modeled is the bombardment of an ethylidyne (C_2H_3) overlayer adsorbed on Pt{111} by a 500-eV Ar atom beam. Approximately 80% of the ejected hydrocarbon species originate from a single C_2H_3 adsorbate, while the others result from reactions between two C_2H_3 adsorbates. A study of the internal energies of all of the ejected hydrocarbon aggregates reveals that those originating from a single C_2H_3 adsorbate are generally stable to any further fragmentation or rearrangement. Examples of common ejection mechanisms for species which originate from a single adsorbate, such as CH_3, C_2H_3, or HCCH, and those which originate from more than one adsorbate, such as CH_4, are given.

Introduction

Presently, molecular dynamics (MD) computer simulations are being used to study a wide variety of events to obtain quantities that can be directly compared with experimental results as well as provide valuable information about the mechanisms and reaction pathways by which these processes occur. The application of such simulations has been ever increasing due to the development of realistic interaction potentials and the increase in computer power. Concomitant with these developments is a push to extend the MD approach into more and more complex processes that embody ensembles of thousands of atoms. It is, in fact, these complex systems where the MD approach can be the vehicle by which the imagination of the scientist is expanded. For example, MD simulations have proposed that tower-like structures that are formed during the etching of silicon by F atoms are the precursors for gaseous products like Si_2F_6 which have more than one Si atom.[1] Subsequent MD simulations have demonstrated that these tower-like structures are easily sheared off by kiloelectronvolt Ar bombardment[2] thus proposing an explanation for the cooperative enhancement of Si removal rate by both halogen reactive etching and particle bombardment.

One fertile testing ground for the molecular dynamics approach is kiloelectronvolt particle bombardment of solids. In this process the energy of the incident particle is many times that of the individual bond strengths and a multitude of reaction channels are accessible.[3−12] It is virtually impossible to guess all the possible pathways and to estimate the importance of each one. Without some concept of what is occurring, it is oftentimes challenging to design experiments to address specific fundamental questions. Since, the MD approach has been quite successful in providing quantitative agreement with experimental energy and angular distributions of single crystal metal and semiconductor systems,[6] it is timely to push it forward to organic films where many more reactions are known to occur. The experimental interest in complex molecular solids such as polymers and biological matrices has been invigorated by recent advances in time-of-flight mass spectrometers, liquid metal ion guns, and ultrafast laser systems.[3,4] It is now possible to image a molecular surface on the 500−1000 Å scale,[13] a dimension that is feasible to model by computer simulations. Moreover with developments in laser postionization approaches, the detected species are ejected as neutral entities rather than ions as is conventionally the case in secondary ion mass spectrometry or fast atom bombardment mass spectrometry. These experimental developments bring closer together the overlap region between experimental reality and computational capability. Since the real experimental systems that we ultimately wish to understand are still more intricate than is feasible to simulate, we start with a realistic prototype in hopes of gaining information about important concepts and classes of mechanisms that can be generalized to complex systems.

In this paper we present a molecular dynamics procedure for the high-energy particle bombardment of a hydrocarbon film adsorbed on a metal substrate. A blended interaction potential which combines a Molière repulsive potential,[14] the embedded atom method Pt potential,[15] Brenner's hydrocarbon potential,[16,17] a Len-

[⊗] Abstract published in *Advance ACS Abstracts,* April 1, 1995.

(1) Schoolcraft, T. A.; Garrison, B. J. *J. Am. Chem. Soc.* **1992,** *113,* 8221.

(2) Feil, H.; Dieleman, J.; Garrison, B. J. *J. Appl. Phys.* **1993,** *74,* 1303.

(3) Winograd, N. *Anal. Chem.* **1993,** *65,* 622A.

(4) Benninghoven, A.; Hagenhoff, B.; Niehuis, E. *Anal. Chem.* **1993,** *65,* 630A.

(5) Leggett, G. J.; Vickerman, J. C. *Int. J. Mass Spectrom. Ion Processes* **1992,** *122,* 281.

(6) Winograd, N.; Garrison, B. J. In *Ion Spectroscopies for Surface Analysis*; Czanderna, A. W., Hercules, D. M., Eds.; Plenum Press: New York, 1991; pp 45−141.

(7) Detter, L. D.; Hand, O. W.; Cooks, R. G.; Walton, R. A. *Mass Spectrom. Rev.* **1988,** *7,* 465.

(8) Sunner, J.; Morales, A.; Kebarle, P. *Int. J. Mass. Spectrom. Ion. Processes* **1988,** *86,* 169.

(9) Pachuta, S. J.; Cooks, R. G. *Chem. Rev.* **1987,** *87,* 647.

(10) Benninghoven, A. *Springer Ser. Chem. Phys.* **1984,** *36,* 342.

(11) Rinehart, K. L., Jr. *Science* **1982,** *218,* 254.

(12) Vickerman, J. C., Brown, A., Reed, N. M., Eds. *Secondary Ion Mass Spectrometry-Principles and Applications;* Oxford University Press: New York, 1989; pp 1−71, 149−243.

(13) Garrison, B. J.; Winograd, N. *CHEMTECH* **1993** (Jan), 25.

(14) The correction to the screening factor in the Molière is given by eq 6 of O'Connor, D. J.; MacDonald, R. J. *Radiat. Eff.* **1977,** *34,* 247. The complete Molière equation is also given herein.

(15) (a) Foiles, S. M.; Baskes, M. I.; Daw, M. S. *Phys. Rev. B* **1986,** *33,* 7983. (b) Daw, M. S.; Baskes, M. I. *Phys. Rev. B* **1984,** *29,* 6443. (c) Daw, M. S.; Baskes, M. I. *Phys. Rev. Lett.* **1983,** *50,* 1285.

0743-7463/95/2411-1220$09.00/0

nard-Jones Pt−H potential,[18] and a Pt−C potential energy function designed to work in conjunction with Brenner's hydrocarbon potential has been developed. This new potential energy function allows the examination of reactions among the various molecular adsorbates. This was not possible with the potential energy functions used in earlier MD studies of the high-energy particle bombardment of organic films on metal substrates.[19,20] With the ability to monitor on an atomic and molecular level what is happening in the film, these simulations form a foundation by which to begin to understand the experimental observables and to move forward to simulations in which additional physical processes such as electronic excitation can be included.

The model system studied is a $p(2\times2)$ overlayer of ethylidyne, C_2H_3, adsorbed on the {111} face of platinum. C_2H_3 is the accepted intermediate through which the Pt catalyzed dehydrogenation of ethylene and acetylene proceeds.[21,22] Because of the technological importance of this reaction, many investigations of the C_2H_3/Pt{111} bonding geometry and strength have been done.[22] C_2H_3 is believed to adsorb in the 3-fold hollow site via three Pt−C bonds with the C−C bond axis perpendicular to the surface. The C_2H_3/Pt system is sufficiently simple to be computationally feasible and yet complex enough to explore possible reaction pathways inherent to the high-energy particle bombardment of molecular films consisting of hydrocarbons.

In general agreement with the experimental investigations of this system,[21] the simulations of 500-eV Ar bombardment of C_2H_3 on Pt{111} predict that the dominant ejected species is the CH_3 fragment, although, many other species are observed. A variety of reaction mechanisms are predicted. One interesting concept is that chemical reactions can occur between species that have been energized by a collision and undisturbed portions of the film to yield molecular species such as CH_4. The initiation of chemical reactions by the surface collision event allows for new ways of thinking about and analyzing the experimental observables.

The methodology and in particular the blending of the various interaction potentials are discussed first. The quantitative results of the calculation are discussed next along with a description of the reaction mechanisms that emerge from the simulations.

Method

As a prototype, the bombardment of a C_2H_3 film adsorbed on Pt{111} with a 500-eV argon beam was chosen for investigation. The classical molecular dynamics scheme being used has been described in extensive detail elsewhere.[23,24] Here, we include many-body potential energy functions which allow for chemical reactions among all of three constituents of the target. Thus, as the collision cascade evolves, reactions occurring among the substrate atoms, the substrate and adsorbate atoms, and the individual adsorbate atoms can be followed in time via the integration of Hamilton's equations of motion. Along with the mechanistic information obtained during the simulation, a variety of experimentally observable properties, such as total particle yield or energy and angular distributions, can be calculated from the final positions and momenta of the ejected particles.

Briefly, the theoretical model consists of approximating the Pt{111} substrate by a finite microcrystallite containing 1512 Pt atoms arranged in seven layers of 216 atoms each. Ethylidyne is alternatively placed in the fcc 3-fold site (i.e., above a third layer Pt atom) or the hcp 3-fold site (i.e., above a second layer atom) in a 0.25 monolayer (ML) $p(2\times2)$ configuration as shown in Figure 1a. For this 1512-atom Pt{111} crystal, 45 C_2H_3 adsorbate molecules placed in the fcc sites or 52 C_2H_3 adsorbate molecules placed in the hcp sites yield the desired 0.25 ML coverage. Since these studies are designed for exploring reaction mechanisms appropriate to a larger class of systems, we chose to investigate a higher coverage (0.50 ML) which has been proposed experimentally[25] and whose density is more representative of polymer films. To obtain a 0.50 ML C_2H_3 coverage, 152 C_2H_3 adsorbates are placed in a honeycomb arrangement above both fcc and hcp 3-fold sites as shown in Figure 1b on a 2310-atom Pt crystal uniformlly distributed in seven layers. The crystal sizes are chosen such that the main dynamical effects of the collisional impact are retained. In all of the simulations, open boundary conditions are used as particles that leave the sides or bottom in reality penetrate deeper into the crystal.[23] Periodic boundary conditions are not appropriate as a particle leaving one side of the crystal should not bring its energy into the other side. Particles should be allowed to exit the bottom for a similar reason.

To mimic experimental conditions, the Ar beam must sample the entire surface or its symmetrical equivalent. For normal incidence of the beam, the appropriate impact zone for a $p(2\times2)$ C_2H_3 film on Pt{111} is shown in Figure 1a. A total of 570 Ar aiming points, or trajectories, were run within this representative area of the surface for each of the 0.25 ML C_2H_3 films discussed above. A total of 250 trajectories were calculated for the 0.50 ML film (Figure 1b). Each trajectory is terminated when the total energy of any atom remaining in the solid falls below the level where any further ejection can take place. This time is typically 0.5−1.5 ps and depends on the aiming point of the Ar and how the energy gets partitioned to the solid and how much escapes. Each trajectory is initiated using a fresh sample with the atoms placed at their equilibrium positions. Thermal motion is not included in the model.

The forces among the target atoms are calculated using a blend of empirical potential energy functions. The Ar−Pt, Ar−C, and Ar−H interactions are described using a purely repulsive Molière pairwise potential energy function.[14] Since the collisions occurring between the impinging Ar atom and the target (the Pt substrate and C_2H_3 film) are energetic in nature and Ar is relatively inert to reactions with Pt, C, and H atoms, this assumption is deemed reasonable. For the remainder of the system, both the repulsive and attractive interactions among the

(16) Brenner, D. W. *Phys. Rev. B* **1990**, *42*, 9458.
(17) Brenner, D. W.; Harrison, J. A.; White, C. T.; Colton, R. J. *Thin Solid Films* **1991**, *206*, 220.
(18) Allen, M. P.; Tildesley, D. J. *Computer Simulation in Liquids*; Oxford University Press: Oxford, 1987; p 9.
(19) (a) Garrison, B. J. *Int. J. Mass Spectrom.* **1983**, *53*, 243. (b) Garrison, B. J. *J. Am. Chem. Soc.* **1982**, *104*, 6211. (c) Garrison, B. J. *J. Am. Chem. Soc.* **1980**, *102*, 6553. (d) Moon, D. W.; Winograd, N.; Garrison, B. J. *Chem. Phys. Lett.* **1985**, *114*, 237.
(20) Lauderback, L. L.; Ang, M. L.; Murray, H. C. *J. Chem. Phys.* **1990**, *93*, 6041.
(21) (a) Creighton, J. R.; White, J. M. *Surf. Sci.* **1983**, *129*, 327. (b) Ogle, K. M.; White, J. M. *Surf. Sci.* **1986**, *165*, 234. (c) Ogle, K. M.; Creighton, J. R.; Akhter, S. A.; White, J. M. *Surf. Sci.* **1986**, *169*, 246.
(22) Starke, U.; Barbieri, A.; Materer, N.; Van Hove, M. A.; Somorjai, G. A. *Surf. Sci.* **1993**, *286*, 1, and references therein.
(23) (a) Harrison, D. E., Jr. *CRC Crit. Rev. Solid State Mater. Sci.* **1988**, *14*, 51. (b) Garrison, B. J. *Chem. Soc. Rev.* **1992**, *21*, 155. (c) Garrison, B. J.; Winograd, N.; Harrison, D. E., Jr. *J. Chem. Phys.* **1978**, *69*, 1440.
(24) (a) Garrison, B. J.; Winograd, N.; Deaven, D. M.; Reimann, C. T.; Lo, D. Y.; Tombrello, T. A.; Harrison, D. E., Jr.; Shapiro, M. H. *Phys. Rev. B* **1988**, *37*, 7197. (b) Bernardo, D. N.; Bhatia, R.; Garrison, B. J. *Comp. Phys. Commun.* **1994**, *80*, 259.
(25) (a) Levis, R.; Winograd, N.; DeLouise, L. A. *J. Am. Chem. Soc.* **1987**, *109*, 6873. (b) Yo, R.; Gustafsson, T. *Surf. Sci.* **1987**, *182*, L234. (c) Freyer, N.; Pirug, G.; Bonzel, H. P. *Surf. Sci.* **1983**, *125*, 327.

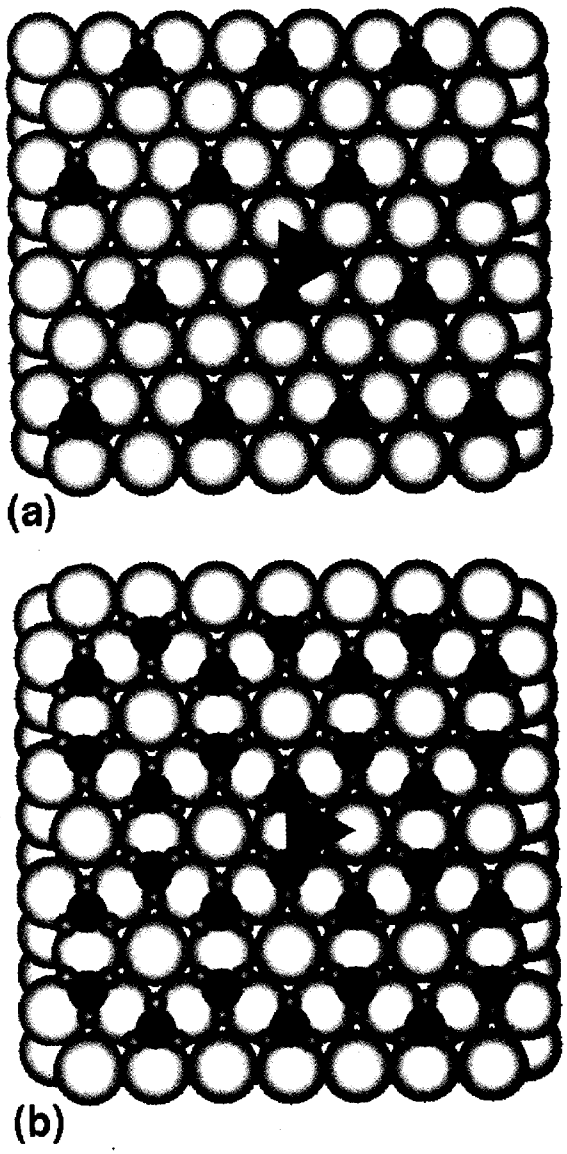

Figure 1. Film configurations for (a) a 0.25 ML C_2H_3 film and (b) a 0.50 ML C_2H_3 film (honeycomb configuration), both arranged in a $p(2\times2)$ overlayer configuration adsorbed on Pt-{111}. The 0.50 ML film has two C_2H_3 adsorbates per unit cell while the 0.25 ML film has only one. The light gray spheres represent Pt atoms, the dark gray spheres represent C atoms, and the medium gray spheres represent H atoms. This color pattern will be repeated in Figures 2, 5, 6, 7, and 8. The impact zone for each film is shown by a triangle.

particles must be described since information about mechanisms of molecule formation and possible reaction pathways is of interest. The Pt−Pt interactions are accounted for by an attractive, many-body potential function based upon the embedded atom method (EAM).[15,24] As described previously,[26] a Molière function has been attached to the EAM repulsive wall to handle the highly energetic collisions which occur between the Pt atoms. The EAM Pt potential was chosen as energy and angular distributions calculated from MD simulations of the high-energy bombardment of other fcc metals using EAM potentials compare well with the corresponding experimental observations.[6,24]

The C−C, C−H, and H−H interactions are described with a reactive many-body potential energy function developed by Brenner.[16,17] Not only are the structures and energetics of bulk diamond and graphite described, but also those of a wide array of small hydrocarbon molecules such as C_2H_4, C_2H_6, and C_6H_6 and radicals such as CH_3 and C_2H_5. This potential[16] was originally developed to model the chemical vapor deposition of diamond films but, in fact, has been used in a number of simulations of other hydrocarbon interactions and reactions including the insertion of CH_2 into a surface dimer on the diamond {001}(2 × 1)H surface,[27] fullerene formation from graphitic ribbons[28] as well as fullerene cage stability,[29] collision and subsequent reactions of fullerenes with a diamond surface,[30] compression of fullerenes between graphitic sheets,[17] the pick-up of a molecule from a surface by another gas-phase molecule (an Eley-Rideal reaction sequence),[31] and compression,[32] indentation,[33] reaction,[34-36] and friction[37] at diamond surfaces. In addition it has been used to generate geometries for subsequent electronic structure calculations.[38]

Although Brenner's model describes well the attractive, or bonding, region of the hydrocarbon potential energy surface, it does not correctly describe the repulsive wall. For instance, the energy of the repulsive wall for the H_2 potential curve at $r_{HH} = 0$ Å is only 48.7 eV. It is possible that the collision cascade initiated by a 500-eV Ar atom could cause two hydrogen atoms to collide with more energy than this, and consequently the atoms would pass through one another. As with the EAM potentials, it is necessary to affix a Molière repulsive wall onto the repulsive part of the H−H potential, and for similar reasons onto the C−H and C−C potentials. This is accomplished via a linear interpolation scheme which uses

(26) Wucher, A.; Garrison, B. J. *Surf. Sci.* **1992**, *260*, 257.

(27) Garrison, B. J.; Dawnkaski, E. J.; Srivastava, D.; Brenner, D. W. *Science* **1992**, *255*, 835.
(28) Robertson, D. H.; Brenner, D. W.; White, C. T. *J. Phys. Chem.* **1992**, *96*, 6133.
(29) Maiti, A.; Brabec, C. J.; Bernholc, J. *Phys. Rev. Lett.* **1993**, *70*, 3023.
(30) Mowrey, R. C.; Brenner, D. W.; Dunlap, B. I.; Mintmire, J. W.; White, C. T. *Mater. Res. Soc. Symp. Proc.* **1991**, *206*, 357. Mowrey, R. C.; Brenner, D. W.; Dunlap, B. I.; Mintmire, J. W.; White, C. T. *J. Phys. Chem.* **1991**, *95*, 7138. Mowrey, R. C.; Brenner, D. W.; Dunlap, B. I.; Mintmire, J. W.; White, C. T. *Physics and Chemistry of Finite Systems: From Clusters to Crystals;* Jena, P., Khanna, S. N., Rao, B. K. Eds.; NATO ASI Series C 374; Kluwer, Dordrecht, 1992; p 1353. Robertson, D. H.; Brenner, D. W.; White, C. T. *Mater. Res. Symp. Proc.*, in press.
(31) Williams, E. R.; Jones, Jr., G. C.; Fang, L.; Zare, R. N.; Garrison, B. J.; Brenner, D. W. *J. Am. Chem. Soc.* **1992**, *114*, 3207.
(32) Harrison, J. A.; Brenner, D. W.; White, C. T.; Colton, R. J. *Thin Solid Films* **1991**, *206*, 213.
(33) Harrison, J. A.; White, C. T.; Colton, R. J.; Brenner, D. W. *Surf. Sci.* **1992**, *271*, 57. Harrison, J. A.; Colton, R. J.; White, C. T.; Brenner, D. W. *Mater. Res. Soc. Symp. Proc.* **1992**, *239*, 573.
(34) Brenner, D. W.; Robertson, D. H.; Carty, R. L.; Srivastava, D.; Garrison, B. J. *MRS Symp. Proc.* **1992**, *278*, 255. Brenner, D. W.; Harrison, J. A. *Am. Ceram. Soc. Bull.* **1992**, *71*, 1821.
(35) Peploski, J.; Thompson, D. L.; Raff, L. M. *J. Phys. Chem.* **1992**, *96*, 8538. Chang, X.; Perry, M.; Peploski, J.; Thompson, D. L.; Raff, L. M. *J. Chem. Phys.* **1993**, *99*, 4748. Chang, X; Thompson, D. L.; Raff, L. M. *J. Chem. Phys.* **1993**, *97*, 10112. Chang, X.-Y.; Thompson, D. L.; Raff, L. M. *J. Chem. Phys.* **1994**, *100*, 1765. Perry, M. D.; Raff, L. M. *J. Phys. Chem.* **1994**, *98*, 4375.
(36) Alfonso, D. R.; Ulloa, S. E. *Phys. Rev. B* **1993**, *48*, 12235. Alfonso, D. R.; Ulloa, S. E.; Brenner, D. W. *Phys. Rev. B* **1994**, *49*, 4948.
(37) Harrison, J. A.; White, C. T.; Colton, R. J.; Brenner, D. W. *Phys. Rev. B* **1992**, *46*, 9700. Harrison, J. A.; White, C. T.; Colton, R. J.; Brenner, D. W. *MRS Bull.* **1993**, *18*, 50. Harrison, J. A.; White, C. T.; Colton, R. J.; Brenner, D. W. *J. Phys. Chem.* **1993**, *97*, 6573. Harrison, J. A.; White, C. T.; Colton, R. J.; Brenner, D. W. *Wear* **1993**, *168*, 127. Sinnott, S. B.; Colton, R. J.; White, C. T.; Brenner, D. W. *Surf. Sci. Lett.*, **1994**, *316*, L1055.
(38) Page, M.; Brenner, D. W. *J. Am. Chem. Soc.* **1991**, *113*, 3270. Dunlap, B. I.; Brenner, D. W.; Mowrey, R. C.; Mintmire, J. W.; Robertson, D. H.; White, C. T. *Mater. Res. Soc. Symp Proc.* **1991**, *206*, 687. Dunlap, B. I.; Brenner, D. W.; Mintmire, J. W.; Mowrey, R. C.; White, C. T. *J. Phys. Chem.* **1991**, *95*, 5763. Robertson, D. H.; Brenner, D. W.; Mintmire, J. W. *Phys. Rev. B* **1992**, *45*, 12592. Lyons, M.; Dunlap, B. I.; Brenner, D. W.; Robertson, D. H.; Mowrey, R. C.; Mintmire, J. W.; White, C. T. *Physics and Chemistry of Finite Systems: From Clusters to Crystals;* Jena, P., Khanna, S. N., Rao, B. K. Eds.; NATO ASI Series C 374; Kluwer, Dordrecht, 1992; p 1347. Dunlap, B. I.; Brenner, D. W.; Schriver, G. W. *J. Phys. Chem.* **1994**, *98*, 1756.

Table 1. Molière Spline Parameters for the Pt EAM and the Hydrocarbon Potentials

	r_1 (Å)	r_2 (Å)	E_1 (eV)	E_2 (eV)
Pt–Pt	1.00	1.30	19.9	111.2
H–H	0.05	0.20	36.2	219.0
C–H	0.10	0.25	118.2	461.0
C–C	0.18	0.44	35.4	917.2

the weighting function, $f_c(r_{ij})$:

$$f_c(r_{ij}) = \frac{1}{2} + \frac{1}{2}\cos\left[\frac{\pi(r_{ij} - r_1)}{(r_2 - r_1)}\right] \quad (1)$$

where r_{ij} is the bond distance between atoms i and j, r_1 is the point at which the function becomes purely Molière in form, and r_2 is the point at which the function is purely Brenner in form. The specific values of r_1 and r_2 used for the three hydrocarbon and the Pt EAM potentials and the energies to which these distances correspond are given in Table 1. The interpolation region for each potential is positioned at a smaller internuclear separation than the respective equilibrium bond distance, consequently, the addition of the Molière wall does not affect the description of the bonding dynamics.

Of note is that only nearest-neighbor interactions are considered in the hydrocarbon potential.[16,17] So while the intramolecular interactions of the individual C_2H_3 adsorbates and the possibilities for reactions among the adsorbates are well described, the intermolecular van der Waals type interactions between the adsorbates are omitted.[39] This should not cause a problem in this study, however, since the hydrocarbon potential is not being used to predict the packing density of the adsorbed C_2H_3 film. Moreover, the collisions of interest here between the molecules are sufficiently energetic that the long-range energies are negligible.

The remaining interactions needed are those between the Pt substrate and the C_2H_3 film. Ideally, both the complex chemistry leading to the formation of C_2H_3 from the reaction of C_2H_4 or C_2H_2 on Pt{111} and the bonding geometry and energetics of C_2H_3 adsorbed on Pt{111} should be described. A Pt–C potential energy function that can do this, however, is not yet available. Fortunately, for modeling high-energy particle bombardment, the ability to describe the chemistry leading to the formation of the adsorbate is not needed to understand the mechanisms leading to the adsorbate's ejection. Both the adsorbate's structure and binding site are assumed prior to the beginning of the simulation. Thus, it is important that the energetics and geometry associated with the chosen structure in a given binding site are correctly described. One of the simplest methods available to describe the Pt–C and Pt–H interactions is a simple pairwise potential function. These, however, will not describe any of the many-body interactions that might occur between Pt and C in a PtC complex. Also, unless somehow informed of each carbon's existing Pt neighbors, Brenner's hydrocarbon potential will predict the gas phase geometry for an adsorbate molecule. For instance, the geometry of a CH_3 adsorbate bound on a Pt{111} surface is predicted to be the same as that of gaseous CH_3, i.e., planar. In an attempt to overcome these difficulties, we merged a Pt–C pairwise potential function with Brenner's many-body hydrocarbon potential function in such a way as to describe the binding site energetics and adsorbate geometries of various small hydrocarbons adsorbed on Pt.

Table 2. Pt–C and Pt–H Lennard-Jones 6/12 Parameters

	σ (Å)	ϵ (eV)	r_1 (Å)	r_2 (Å)
Pt–H	1.90	0.88	2.00	2.70
Pt–C	2.20	2.30	2.30	3.00

The Pt–C and Pt–H pairwise interactions have been chosen to be Lennard-Jones potential functions.[18] To ease the merging of the Pt–C pair potential with the hydrocarbon potential, only the nearest neighbor Pt–C and Pt–H interactions are taken into account. This potential can be written as

$$E_{tot} = \sum_{i<j}\left\{f_c(r_{ij})\epsilon\left[\left(\frac{\sigma}{r_{ij}}\right)^{12} - 2\left(\frac{\sigma}{r_{ij}}\right)^{6}\right]\right\} \quad (2)$$

where r_{ij} is the bond distance between atoms i and j, and f_c, which limits the potential to only nearest-neighbor interactions, is given in eq 1 above. Brenner's hydrocarbon potential can be written as follows[16]

$$E_{tot} = \sum_i \sum_{j>i} \{f_c(r_{ij})[V_R(r_{ij}) - \bar{B}(r_{ij},r_{ik},\theta_{jik})V_A(r_{ij})]\} \quad (3)$$

where r_{ij} is the i–j bond distance, V_R and V_A are exponential functions used to calculate the repulsive and attractive pairwise interactions, f_c is a cutoff function used to limit the potential to only nearest-neighbor interactions, and $\bar{B}(r_{ij},r_{ik},\theta_{jik})$ is a many-body coupling of the i–j and j–i bonds which measures the bonding environments of atoms i and j. To correctly calculate $\bar{B}$, the coordinates and identities of all of the neighbors of atoms i and j must be known. If the Pt atoms bound to each hydrocarbon adsorbate are not included in the calculation of the C atom's energy as mentioned above, a physically incorrect structure will be predicted for the adsorbate molecule. Consequently in calculating $\bar{B}$, we chose to treat the Pt atoms as if they were H atoms. This assumes that all of the Pt–C bonds are σ-like, and not π-like, in character. The pairwise quantities, V_R and V_A, are only calculated between hydrocarbon neighbors, but when the bonding environment, $\bar{B}(r_{ij},r_{ik},\theta_{jik})$, of atom i (where i is a C atom) is calculated, all of it neighbors regardless of whether they are H, C, or Pt are included. The Lennard-Jones parameters for Pt–C have been fit to the Pt–CH_3 calculated bond strength of 2.30 eV,[40] and the estimated covalent Pt–C bond length of 2.20 Å.[41] The Pt–H bond length of 1.90 Å is taken from an experimental determination of the H–Pt{111} geometry.[42] The Pt–H bond strength is chosen so that the heat of adsorption is within the range of experimental values.[41,43] All parameters for the Lennard-Jones parameters are given in Table 2. Of note is that the main goal of this study is to examine the overlayer reactions and not reactions of the hydrocarbons with the metal substrate. In the authors opinion, to do the latter will require a different functional form.

In agreement with both the experimental and theoretical data, our merged potential preferentially adsorbs C_2H_3 in a 3-fold hollow site on Pt{111} with its C–C bond axis perpendicular to the surface plane.[21,22] The inclusion in Brenner's hydrocarbon potential of the three Pt atoms

(39) Conversely molecular mechanics type potentials which include the long range interactions do not allow reactions among the molecules to occur. A merging of the two types of potentials is, of course, desirable but not readily available.

(40) Low, J. J.; Goddard, W. A. *J. Am. Chem. Soc.* **1986**, *108*, 6115.
(41) Somorjai, G. A. *Chemistry in Two Dimensions: Surfaces;* Cornell University Press: Ithaca, NY, 1981.
(42) Sayers, C. M. *Surf. Sci.* **1984**, *143*, 411.
(43) Carter, E. A.; Koel, B. E. *Surf. Sci.* **1990**, *226*, 339.

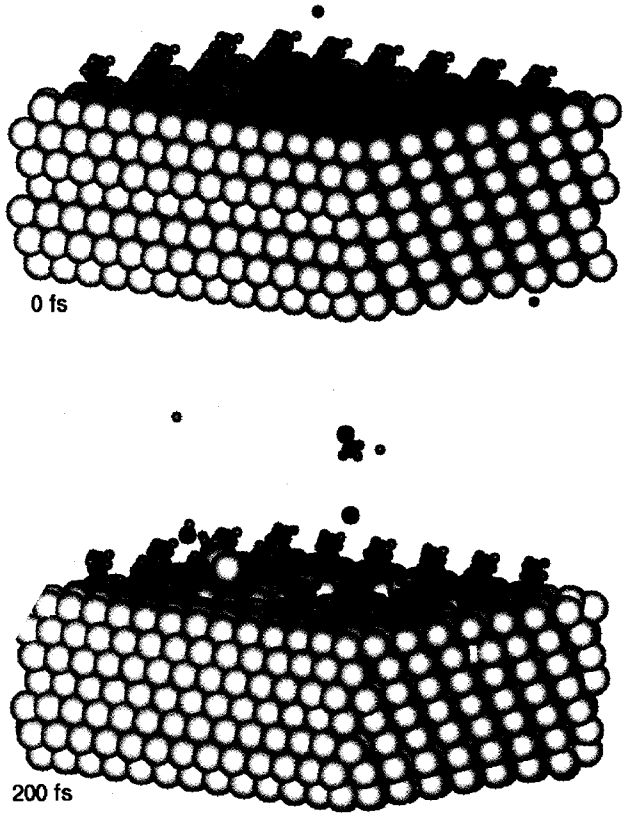

Figure 2. Example trajectory calculated for the 500-eV Ar bombardment of a 0.25 ML C_2H_3 film adsorbed on Pt{111}. Frame 1 is prior to the Ar atom bombardment. As shown in Frame 2, 200 fs into the trajectory, Pt, H, C, CH_2, and an C_2H_3 adsorbate are leaving the crystal.

bound to each C_2H_3 adsorbate results in a 1.92 eV stabilization in energy of the C_2H_3 structure, which otherwise would be that of a C_2H_3 radical. Each Pt–C bond is 0.15 eV stronger than that predicted by the Lennard-Jones potential described above for a single C atom adsorbed on Pt. Thus, each C_2H_3 adsorbate has a total binding energy to the surface of 7.35 eV which is well within the reported range of 6.9–8.8 eV.[41,43] Although experiments suggest that C_2H_3 prefers the fcc to the hcp 3-fold site,[22] this potential predicts there to be no difference between the binding energies of the two sites. As discussed later this does not affect the mechanisms of organic molecule formation. Unlike a simple pairwise potential, our merged potential does not predict the 3-fold site to be the most stable site for all CH_x adsorbates. Instead, an adsorbate will bind in the site which allows the binding C atom to attain a 4-fold coordination. For example, on Pt{111}, CH_3 preferentially binds in the atop site, CH_2 binds in the 2-fold bridge site, and CH and C_2H_3 bind in the 3-fold hollow site. Although, these structures are intuitive, no definitive measurements have been made for any of the CH_x adsorbates.

Results and Discussion

In a typical collision event, both atoms and molecular aggregates[44] are ejected from the crystal into the vacuum. For instance, 200 fs after the start of the trajectory shown in Figure 2, Pt, H, C, CH_2, and the intact adsorbate molecule, C_2H_3, are observed above the surface. In the following sections, we discuss the types of species ejected with C_2H_3 adsorbed in the two 0.25 ML $p(2\times2)$ configurations and compare these with those obtained for the higher density C_2H_3 film and to the available experimental data. The internal energies of the ejected aggregates and possible reaction mechanisms for the formation of CH_3, HCCH, and CH_4 are also discussed. The results that we have chosen to highlight below are those that we feel exhibit concepts that are transferable to a wider range of experimental configurations.

Comparison of Ejected Species. Calculated mass distributions are determined by counting the neutral species which exist 1–2 ps after the bombardment event. We have not attempted to account for experimental factors of ionization probability, ion stability, or possible further fragmentation of the larger species during their microsecond flight to the detector. For convenience the calculated distributions are plotted as "mass spectra". This graphical representation provides a starting point for identifying dominant results for mechanistic analysis. The results for the 500-eV Ar bombardment of the $p(2\times2)$ overlayer of C_2H_3 bound in the fcc 3-fold site are shown in Figure 3a. The results for C_2H_3 placed in the hcp 3-fold site show a similar fragmentation pattern. The total atomic yields of these two C_2H_3 configurations, given in Table 3, are within the statistical error of the simulations, except for the slightly lower yield of H obtained with C_2H_3 placed in the hcp site. No discernible differences are found between the two adsorption sites with regard to the mechanisms of aggregate formation or the distribution of internal energy within the aggregates. Slight differences in energy and angular distributions, however, are found.

An expansion of the low mass region of Figure 3a is shown in Figure 3b. The dominant peak is that of H. A study of the individual trajectories reveals that the ejection of H can result from the direct cleavage of a C–H bond by an energized particle such as the incoming Ar atom or an ejecting Pt, C, H, or C_xH_y species or from the unimolecular dissociation of an unstable C_xH_y after it has been ejected. Of note is that in both scenarios, the fragmentation occurs within the first 1–2 ps of the Ar impact. An estimate of fragmentation that will occur during the microseconds flight to the detector is given below. In agreement with the experimental findings,[21] these calculations predict the detection of more C_1 than C_2 hydrocarbons, with CH_3 being the most intense. A common mechanism leading to the ejection of CH_3 is discussed below. Although organic molecules with more than two C atoms are ejected, the yield of the most abundant of these, C_3H_3, is <0.02% of the H yield.

High-Density C_2H_3 Overlayer. The results obtained from the 0.5 ML film are shown in Figure 3c, and in comparison to the 0.25 ML $p(2\times2)$ configuration, the honeycomb configuration results in twice as many hydrocarbon species being ejected. Fewer Pt atoms are ejected when the film density is increased. This is reflected in the total atomic yields given in Table 3. Although more H_2 and CH_4 are predicted to eject (Figure 3d), the results are similar to that of the less dense film with the H and CH_3 species being the most probable. (The C_2 region in Figure 3d is slightly different from that of Figure 3b.) Of note is that neither H_2 nor CH_4 exists on the surface prior to the Ar bombardment; thus they must be a product of a chemical reaction initiated by the bombardment event. Not surprisingly the probability that two entities will come together and react increases with increasing film density. This is also the reason for the larger C_2H_2 and $C_2H_{x(x\geq4)}$ intensities than found for the 0.25 ML simulations. Although the yield is higher and the variety of species more extensive for the 0.50 ML film than for the 0.25 ML film, the mechanisms of molecule formation are the same. The more common ones of these are discussed below.

(44) It is not clear what to call these entities. They are not real molecules in that many will dissociate. The cluster scientists object to these being called clusters although in fact they are clusters of atoms.

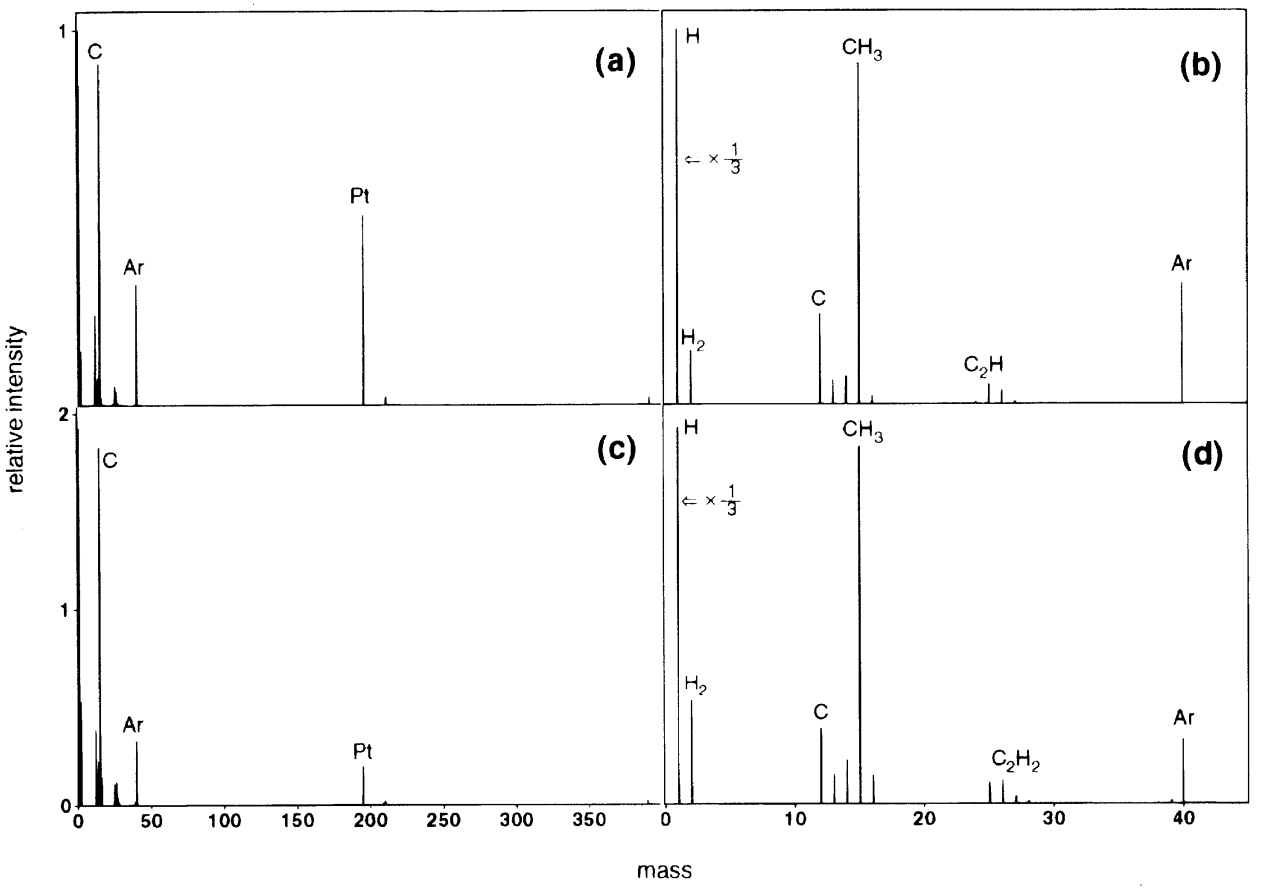

Figure 3. Calculated results. (a) 0.25 ML film with C_2H_3 adsorbed in fcc 3-fold sites in a $p(2\times2)$ configuration as shown in Figure 1a. (b) Expansion of the low mass region of (a). (c) 0.50 ML film with C_2H_3 adsorbed in honeycomb configuration as shown in Figure 1b. (d) Expansion of the low mass region of (c). The peaks in (a) and (b) range in intensity from 0 to 1, while the peaks in (c) and (d) range in intensity from 0 to 2. The normalizations are internally consistent so that direct comparisons can be made. The intensity at 39.9 amu corresponds to those incident Ar atoms which are reflected back into the vacuum after having imparted a portion of their initial energy into the crystal.

Table 3. Total Atomic Yields per Incident Ar Particle for the Three Different C_2H_3 Films

	fcc 0.25 ML	hcp 0.25 ML	honeycomb 0.50 ML
H	13.0	11.7	22.2
C	3.2	3.2	6.0
Pt	1.2	1.1	0.5
Ar	0.6	0.7	0.7

Observable $PtCH_3$ intensities are shown in parts a and c of Figure 3. At this stage the specifics of the potential surfaces including the binding energies for the gas phase $PtCH_x$ species are unknown; thus a detailed analysis is not warranted. As a reference point the interaction potential that we are using has a binding energy of 2.3 eV between the Pt and hydrocarbon species.

Distribution of Internal Energy. Experimentally it is the molecules (neutral or ionic) that survive for at least a microsecond after the particle bombardment event which are detected. In this vein we are interested in how many of the ejected species will remain intact for the microsecond duration necessary for them to be experimentally observed. As an indicator of stability we define the effective internal energy, E_{eff}, of each group of atoms as follows:

$$E_{\text{eff}} = V(r_{ij}) + \text{ke}(r_{ij}) - V_{\text{eq}} - E_{\text{dissoc}} \qquad (4)$$

where $V(r_{ij})$ and $\text{ke}(r_{ij})$ are the potential and kinetic energy relative to the center of mass calculated from atomic coordinates and velocities at the termination of the collision cascade, V_{eq} is the equilibrium potential energy,

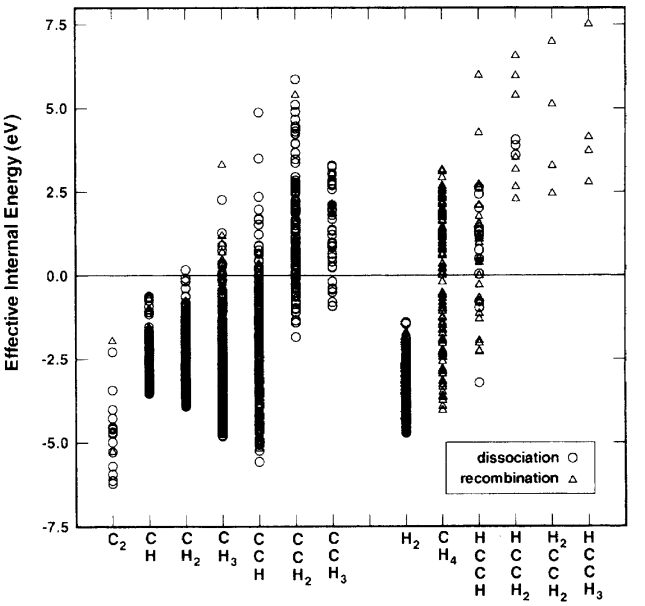

Figure 4. Effective internal energies of aggregates ejected in the 500-eV Ar bombardment of the two 0.25 ML C_2H_3 films and the 0.50 ML film. Those indicated with a "○" originate from a single C_2H_3 adsorbate, while those indicated with a "△" consist of atoms from two C_2H_3 adsorbates. An effective internal energy below 0 eV indicates that no further fragmentation or rearrangement of the cluster will occur.

and E_{dissoc} is the lowest bond dissociation energy as predicted by Brenner's hydrocarbon potential. Figure 4

Table 4. Total Yield of $C_{x(x=0-2)}H_{y(y=0-4)}$ Species Which Result from the 500-eV Ar Bombardment of the Two 0.25 ML and One 0.50 ML C_2H_3 Films

aggregate	no. formed	% originating from single adsorbate	% stable against further fragmentation
	Dissociation of Single Adsorbate		
C_2	17	88	100
CH	208	82	100
CH_2	291	93	100
CH_3	2838	98	99
CCH	173	81	87
CCH_2	113	88	25
CCH_3	38	90	18
	Recombination of Two Adsorbates		
H_2	538	30	100
CH_4	115	0	41
HCCH	38	34	32
$HCCH_2$	10	30	0
H_2CCH_2	4	0	0
$HCCH_3$	4	0	0

shows the effective internal energy calculated for the $C_{x(x=0-2)}H_{y(y=0-4)}$ species which are ejected. Since there does not appear to be a dependence on either the binding site or the density of the adsorbate film, Figure 4 and Table 4 contain all of the species ejected in the simulations of both the 0.25 ML and the 0.50 ML C_2H_3 films. The composition is shown along the x-axis. In both Figure 4 and Table 4, the species are grouped according to their origin. The first grouping contains those species such as CH, CH_3, and C_2H_3 which are primarily products of the dissociation or fragmentation of a single C_2H_3 adsorbate. The second grouping contains those which form primarily through the reaction of two or more adsorbates. The percentage of each type resulting from the dissociation of a single C_2H_3 adsorbate is also given in Table 4. Concentrating first on the grouping that arises primarily from a single C_2H_3 species, most aggregates are stable with respect to further fragmentation. The exceptions are CCH_2 (as distinguished from HCCH) and CCH_3 both of which have low (2 eV) dissociation energies. Almost all of the species arising from two adsorbates are unstable with respect to further fragmentation except H_2, CH_4, and HCCH. Given that all three of these molecules are experimentally known to be very stable, it is reassuring that the potential predicts a relatively high stability for each. The 0.50 ML simulations result in more species which originate from two rather than only one C_2H_3 molecule.

There are well-developed prescriptions for modeling the unimolecular decomposition and rearrangement of excited molecules,[45] one of which has been used to estimate the decomposition of Ag clusters ejected in MD calculations of kiloelectronvolt particle bombardment.[46] At this stage we do not feel that the quality of the interaction potential being used justifies such a detailed analysis. Moreover, many experiments detect the ions that are ejected and one must then describe the decomposition of the ionic and not the neutral species. Suffice it to say that virtually all of the particles shown in Figure 4 with effective internal energies greater than 0 eV will decompose.

Mechanisms. As shown in Figures 3 and 4, a variety of species are created during the collision event. Often these are merely a portion of the molecular adsorbate, e.g., CH_3, CCH, CCH_2, or even the intact C_2H_3. Occasionally, however, species which show little structural relationship to the C_2H_3 adsorbate are detected, e.g., H_2, CH_4, or HCCH. Understanding the mechanisms that lead to the formation of the different species provides alternative explanations for peaks typically observed in experimental spectra. Examples of the more common mechanisms as predicted by our calculations are discussed below.

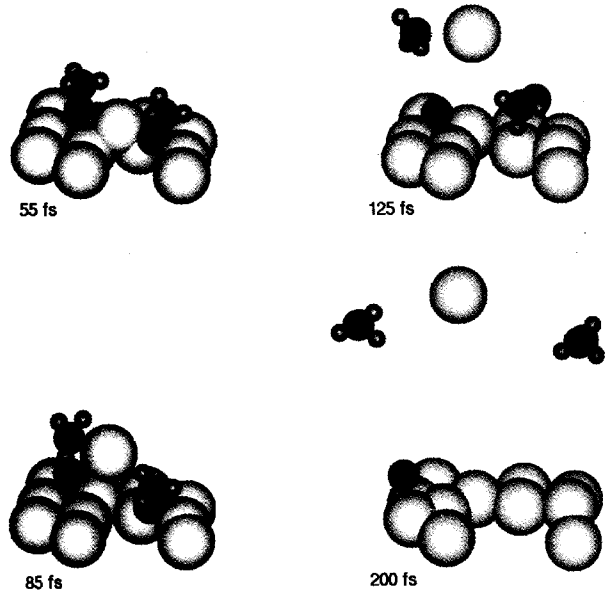

Figure 5. Ejection of both a portion of an intact C_2H_3 adsorbate and an entire C_2H_3 adsorbate. In the 55-fs frame, the C_2H_3 adsorbate on the left desorbs as CH_3 and a C atom, while the C_2H_3 adsorbate on the right desorbs intact.

Ejection of a Portion of the Intact Adsorbate. The most common mechanism of ejection observed in these calculations is the fragmentation of a single C_2H_3 adsorbate. This process usually results from the direct collision of either the bombarding particle or a moving C_xH_y or Pt particle with an C_2H_3 adsorbate. Figure 5 shows one of the more common mechanisms for the formation of CH_3 which is the dominant species formed via this type of mechanism. Less than 40 fs into the collision event, a second layer Pt atom collides with a first layer Pt atom causing the upward motion of the first layer Pt atom. As the Pt atom tries to leave the surface region, it collides with an C_2H_3 adsorbate, breaking the C−C bond and releasing CH_3. This whole process takes less than 85 fs and in this case results in a C atom remaining adsorbed to the surface, a free CH_3 radical, and a free Pt atom.

Also shown in the specific collision sequence shown in Figure 5 is the ejection of an intact C_2H_3 adsorbate. This C_2H_3 adsorbate is bound to the first layer Pt atom which gets struck from below by a second layer Pt atom. The momentum of the first layer Pt atom is moving it away from, and not directly into, the C_2H_3 adsorbate. Instead of the C_2H_3 adsorbate fragmenting, it is ejected from, *or rolled off of*, the surface intact. In contrast, when the momentum of the ejecting Pt atom is directed toward the C_2H_3 adsorbate, the molecule usually undergoes fragmentation and/or rearrangement.

The mechanisms discussed above are not specific to the formation of CH_3 and CCH_3. Other species originating from a single adsorbate are often formed via similar mechanisms. If the energy of the colliding particle is high or it strikes the C_2H_3 adsorbate in close proximity to a H atom, a CH_2 or CH species might result. C_2H_3 adsorbates often undergo collisions which result in the ejection of a CCH_2 species and a H atom. Mechanisms of this type make possible the direct mapping of the experimental observables to the chemical/structural properties of the adsorbate film.

(45) Robinson, P. R.; Holbrook, *Unimolecular Reactions*; Wiley: London, 1972.
(46) Wucher, A.; Garrison, B. J. *Phys. Rev. B* **1992**, *46*, 4855.

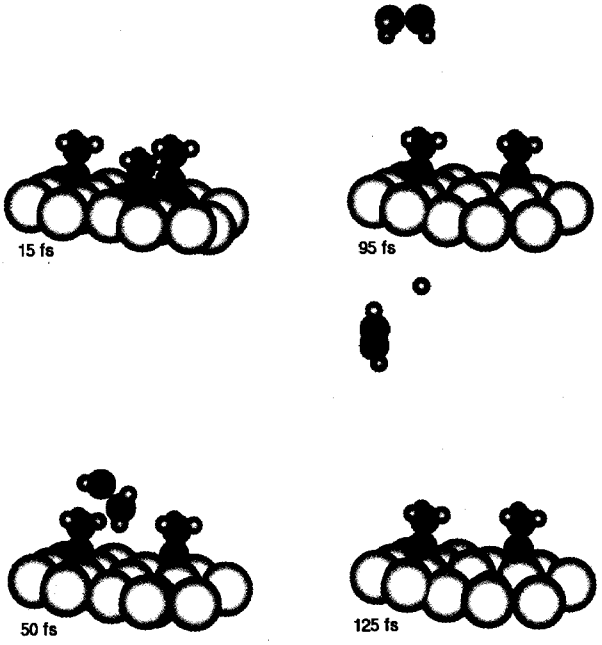

Figure 6. Unimolecular rearrangement and fragmentation of C_2H_3 yielding HCCH.

Unimolecular Dissociation and Rearrangement. Often before reaching the detector, ejected CCH_3 clusters undergo rearrangement and/or fragmentation to yield products such as H_2, CCH_2, CCH, HCCH, or H_2CCH. An example of rearrangement and fragmentation is the formation of HCCH as shown in Figure 6. At 15 fs into the simulation, the incoming Ar atom collides with the Pt surface. As the Ar atom penetrates the surface, it pushes a Pt atom in the direction of the C_2H_3 adsorbate to which it is bound. This results in the ejection of the C_2H_3 adsorbate. In contrast to the ejection mechanism discussed above, the C_2H_3 tumbles off of the surface end-over-end. During this tumbling, one of the H atom migrates to the opposite C atom giving a $HCCH_2$ species. At 95 fs, this species is intact but has considerable internal energy. Finally 30 fs later, the $HCCH_2$ ejects a H atom yielding a stable HCCH molecule and a free H atom. Although the potential energy function used to describe the hydrocarbon interactions in these calculations may not predict the correct energy barrier for this reaction, the potential does allow classical dynamics simulations, for the first time, to be used in the qualitative study of the occurrence of unimolecular dissociation/rearrangement-type reactions in the kiloelectronvolt particle bombardment of an organic film. In this example the rearrangement process occurs within the first few hundred femtoseconds of the collision cascade.

Reactions between Molecules. The calculations also predict the occurrence of molecules like methane which cannot form from a single C_2H_3 adsorbate. Two possible mechanisms for the formation of CH_4 are shown in Figures 7 and 8. Both involve the release of a CH_3 radical and its subsequent reaction with a hydrogen atom. These reactions are analogous to the hydrogen abstraction-type mechanism discussed in an earlier paper[47] in which a free H atom is channeled across the surface and subsequently abstracts another H atom from an undisturbed C_2H_3 adsorbate to form H_2. A similar reaction sequence is shown in Figure 7 in which the incoming Ar atom strikes a C_2H_3 adsorbate and causes the ejection of both a free C atom and a CH_3 radical. The CH_3 radical is channeled across the surface where it collides with an undisturbed C_2H_3 adsorbate. The collision results in the abstraction of a H atom from the C_2H_3 adsorbate. The final products are a free CH_4 molecule and an adsorbed C_2H_2 species. In this example the attacking CH_3 radical is oriented such that the C atom end collides with the C_2H_3. When the angle of the attacking CH_3 molecule is such that a H atom is the first to react with the C_2H_3 adsorbate, H abstraction does not occur. Instead, depending upon the energy of the incoming CH_3 radical, the C–H bond on the C_2H_3 adsorbate may break to create a free H atom or the C–C bond might break to give a second CH_3 species.

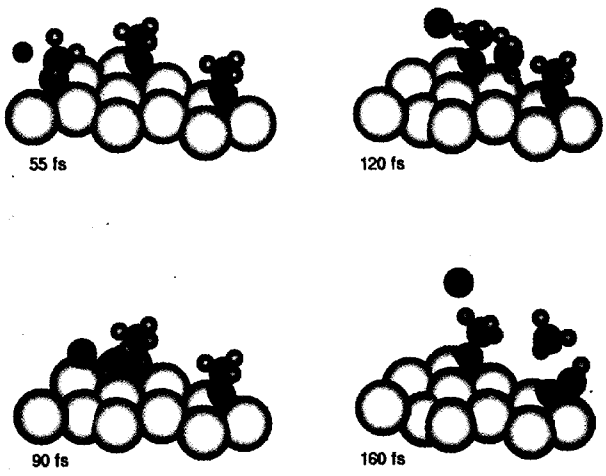

Figure 7. Hydrogen abstraction reaction by a free CH_3 radical which leads to the formation of CH_4. The CH_3 radical results from the collision of the incoming Ar atom with the C_2H_3 adsorbate on the left. A H atom is abstracted from the C_2H_3 adsorbate on the right.

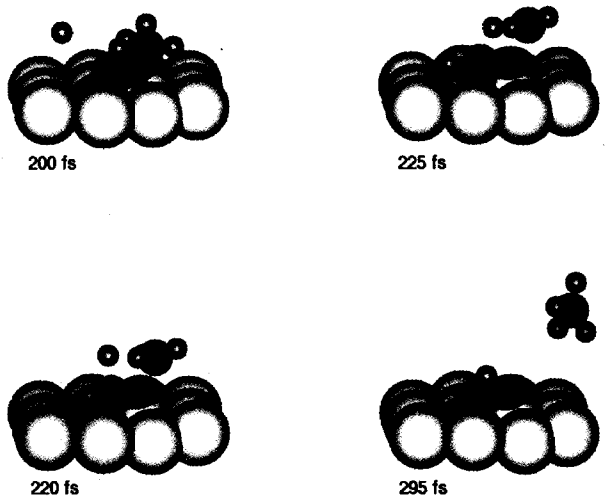

Figure 8. Reaction between a free CH_3 radical and free H atom that results in the formation CH_4. The free CH_3 radical results from the collision of an ejecting CH fragment with the C_2H_3 adsorbate on the right. The H atom results from a collision which occurred in a neighboring portion of the crystal.

The second CH_4 reaction is between a free H atom and a *freshly detached* CH_3 radical (Figure 8). In this example the release of a CH_3 radical is caused by the collision of an ejecting CH_3 species and an C_2H_3 adsorbate. Before the CH_3 species can escape the surface region, it collides with a free H atom created earlier in the collision event. These two species react to form CH_4. Collisions between escaping C_xH_y species and free H atoms are not common. Free H atoms are generally created early in the collision event[48] and, given their light mass, are usually well above

(47) Taylor, R. S.; Garrison, B. J. *J. Am. Chem. Soc.* **1994**, *116*, 4465.

(48) Brenner, D. W.; Garrison, B. J. *Phys. Rev. B* **1986**, *34*, 5782.

the surface before there is time to react with anything else.

Although both examples given above only depict the formation of CH_4, as shown in Table 4 chemical reactions are responsible for the formation of some fraction of all of the predicted species including many that are stable against further fragmentation. As must be the case, all of the predicted CH_4, H_2CCH_2, and $HCCH_3$ species are products of the reaction of two adsorbates. Also, this mechanism is responsible for the formation of over half of the predicted H_2, HCCH, and $HCCH_2$ species. The reaction need not be between a H atom and an ejecting CH_y species. It may instead be between two ejecting CH radicals to form HCCH or between an ejecting CH_2 fragment and a bound C_2H_3 adsorbate to form H_2CCH_2.

There is often a question of energy removal during reactions as described above.[19,23] Any collision that occurs where one collision partner is still adsorbed to the surface has numerous vibrational channels which can absorb excess energy. Moreover, the making of one bond, e.g., H_2, often results in the breaking of another bond, e.g., C−H, thus the overal reaction is only exothermic by fractions of a bond strength. Even the reactions between the two "free" collision partners are taking place very near the surface and have ample opportunity to release excess energy.

Conclusions

A many-body Pt−C potential energy function that blends smoothly with Brenner's reactive hydrocarbon and the EAM Pt potential energy functions has been constructed so that molecular dynamics calculations of the kiloelectronvolt particle bombardment of organic films can be performed. The use of reactive potential energy functions to describe the interactions among all of the target atoms allows a microscopic view of reaction mechanisms among the organic overlayer molecules.

Molecular dynamics calculations of the kiloelectronvolt particle bombardment of both 0.25 ML and 0.50 ML $p(2\times2)$ C_2H_3 overlayers adsorbed on Pt{111} have been performed. In general agreement with the experimental findings,[21] these calculations predict the peaks in the C_1 region of the mass spectra to be more intense than those in the C_2 region with the predominant hydrocarbon species being CH_3. Although calculations performed with C_2H_3 adsorbed in the fcc and the hcp sites in a $p(2\times2)$ configuration show slight differences in atomic yields and angular distributions, the mechanisms of product formation are the same. As the film density is increased from 0.25 to 0.50 ML, the abundance of products also increases, but the mechanisms remain the same as those found for the lower density films.

Although a majority of the detected species result from the dissociation of a single C_2H_3 adsorbate, some result from the reaction of two adsorbates in the near surface region. Calculations of the effective internal energies of the predicted species show that those which result from the dissociation of a single adsorbate (i.e., CH_3, CH_2, and C_2H_3) are generally quite stable to further fragmentation. Those species which are produced from the collision-induced reaction of two adsorbates (i.e., H_2, CH_4, and $HCCH_3$), however, tend to be candidates for further fragmentation as they have considerable internal energy. Molecules such as CH_4 can result from both the reaction of a previously ejected entity, i.e., CH_3, either with another free species or with an undisturbed C_2H_3 adsorbate. Molecules such as H_2 and HCCH are found to result from both the dissociation of a single adsorbate and the reaction of two adsorbates.

A method is now available to explore the mechanisms of molecular ejection for organic films adsorbed on surfaces. An atomic view of the processes which lead to the ejection of the intact adsorbate, a portion of the adsorbate, or some entity which was not originally a part of the film allows a clearer understanding of what information the experimental observables contain about the chemical nature of the original film. Future work on understanding how the ionization process affects these mechanisms should bolster our overall understanding of the high-energy bombardment of molecular films.

Acknowledgment. The financial support of the National Science Foundation and the IBM Selected University Research Program is gratefully acknowledged. The Pennsylvania State University supplied a generous grant of computer time for these calculations. We thank Nicholas Winograd, Donald W. Brenner, David E. Sanders, and John C. Vickerman for insightful discussions.

LA9409687